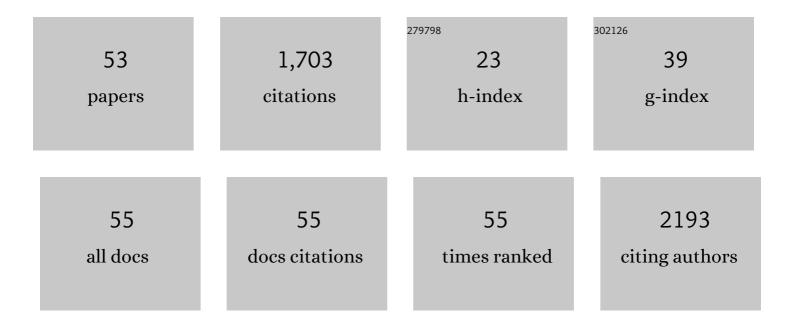
## Basavaraju G Sanganahalli

List of Publications by Year in descending order

Source: https://exaly.com/author-pdf/2802568/publications.pdf

Version: 2024-02-01



#	Article	IF	CITATIONS
1	Negative BOLD with Large Increases in Neuronal Activity. Cerebral Cortex, 2008, 18, 1814-1827.	2.9	207
2	Energetics of neuronal signaling and fMRI activity. Proceedings of the National Academy of Sciences of the United States of America, 2007, 104, 20546-20551.	7.1	121
3	Where fMRI and Electrophysiology Agree to Disagree: Corticothalamic and Striatal Activity Patterns in the WAC/Rij Rat. Journal of Neuroscience, 2011, 31, 15053-15064.	3.6	115
4	Decreased Subcortical Cholinergic Arousal in Focal Seizures. Neuron, 2015, 85, 561-572.	8.1	99
5	Lactate preserves neuronal metabolism and function following antecedent recurrent hypoglycemia. Journal of Clinical Investigation, 2013, 123, 1988-1998.	8.2	80
6	Oxidative Neuroenergetics in Event-Related Paradigms. Journal of Neuroscience, 2009, 29, 1707-1718.	3.6	62
7	Quantitative basis for neuroimaging of cortical laminae with calibrated functional MRI. Proceedings of the National Academy of Sciences of the United States of America, 2013, 110, 15115-15120.	7.1	57
8	Decreased Resting Functional Connectivity after Traumatic Brain Injury in the Rat. PLoS ONE, 2014, 9, e95280.	2.5	54
9	Pitfalls in fractal time series analysis: fMRI BOLD as an exemplary case. Frontiers in Physiology, 2012, 3, 417.	2.8	52
10	Fractal analysis of spontaneous fluctuations of the BOLD signal in rat brain. NeuroImage, 2011, 58, 1060-1069.	4.2	48
11	Afatinib plus Cetuximab Delays Resistance Compared to Single-Agent Erlotinib or Afatinib in Mouse Models of TKI-NaÃ־ve EGFR L858R-Induced Lung Adenocarcinoma. Clinical Cancer Research, 2016, 22, 426-435.	7.0	46
12	Frequencyâ€dependent tactile responses in rat brain measured by functional MRI. NMR in Biomedicine, 2008, 21, 410-416.	2.8	45
13	Increased resting functional connectivity in spikeâ€wave epilepsy in <scp>WAG</scp> / <scp>R</scp> ij rats. Epilepsia, 2013, 54, 1214-1222.	5.1	39
14	Mitochondrial Calcium Uptake Capacity Modulates Neocortical Excitability. Journal of Cerebral Blood Flow and Metabolism, 2013, 33, 1115-1126.	4.3	38
15	Cerebral oxygen demand for shortâ€ŀived and steadyâ€state events. Journal of Neurochemistry, 2009, 109, 73-79.	3.9	35
16	Neurovascular and neurometabolic couplings in dynamic calibrated fMRI: transient oxidative neuroenergetics for block-design and event-related paradigms. Frontiers in Neuroenergetics, 2010, 2, .	5.3	31
17	DYNAmic Multiâ€coll TEchnique (DYNAMITE) shimming of the rat brain at 11.7 T. NMR in Biomedicine, 2014, 27, 897-906.	2.8	30
18	Multimodal Measurements of Blood Plasma and Red Blood Cell Volumes during Functional Brain Activation. Journal of Cerebral Blood Flow and Metabolism, 2009, 29, 19-24.	4.3	29

#	Article	IF	CITATIONS
19	Functional MRI and neural responses in a rat model of Alzheimer's disease. NeuroImage, 2013, 79, 404-411.	4.2	29
20	Analysis of Time and Space Invariance of BOLD Responses in the Rat Visual System. Cerebral Cortex, 2013, 23, 210-222.	2.9	28
21	Brain region and activity-dependent properties of M for calibrated fMRI. NeuroImage, 2016, 125, 848-856.	4.2	26
22	APOE genotype-dependent pharmacogenetic responses to rapamycin for preventing Alzheimer's disease. Neurobiology of Disease, 2020, 139, 104834.	4.4	26
23	Tactile and Non-tactile Sensory Paradigms for fMRI and Neurophysiologic Studies in Rodents. Methods in Molecular Biology, 2009, 489, 213-242.	0.9	26
24	Mitochondrial Functional State Impacts Spontaneous Neocortical Activity and Resting State fMRI. PLoS ONE, 2013, 8, e63317.	2.5	24
25	Metabolic demands of neural-hemodynamic associated and disassociated areas in brain. Journal of Cerebral Blood Flow and Metabolism, 2016, 36, 1695-1707.	4.3	24
26	Quantitative $\hat{I}^2$ mapping for calibrated fMRI. NeuroImage, 2016, 126, 219-228.	4.2	24
27	Glutamate-induced differential mitochondrial response in young and adult rats. Neurochemistry International, 2004, 44, 361-369.	3.8	23
28	Hypofrontality and Posterior Hyperactivity in Early Schizophrenia: Imaging and Behavior in a Preclinical Model. Biological Psychiatry, 2017, 81, 503-513.	1.3	22
29	The Stroke Preclinical Assessment Network: Rationale, Design, Feasibility, and Stage 1 Results. Stroke, 2022, 53, 1802-1812.	2.0	22
30	Differential effects of tricyclic antidepressant drugs on membrane dynamics—a fluorescence spectroscopic study. Life Sciences, 2000, 68, 81-90.	4.3	20
31	New horizons in neurometabolic and neurovascular coupling from calibrated fMRI. Progress in Brain Research, 2016, 225, 99-122.	1.4	19
32	Comparison of glomerular activity patterns by fMRI and wide-field calcium imaging: Implications for principles underlying odor mapping. NeuroImage, 2016, 126, 208-218.	4.2	19
33	Orthonasal versus retronasal glomerular activity in rat olfactory bulb by fMRI. NeuroImage, 2020, 212, 116664.	4.2	19
34	Xanthine oxidase, nitric oxide synthase and phospholipase A2 produce reactive oxygen species via mitochondria. Brain Research, 2005, 1037, 200-203.	2.2	18
35	Kaempferol Treatment after Traumatic Brain Injury during Early Development Mitigates Brain Parenchymal Microstructure and Neural Functional Connectivity Deterioration at Adolescence. Journal of Neurotrauma, 2020, 37, 966-974.	3.4	15
36	Distribution of temperature changes and neurovascular coupling in rat brain following 3,4-methylenedioxymethamphetamine (MDMA, "ecstasyâ€) exposure. NMR in Biomedicine, 2015, 28, 1257-1266.	2.8	14

#	Article	IF	CITATIONS
37	Role of mitochondrial calcium uptake homeostasis in resting state fMRI brain networks. NMR in Biomedicine, 2015, 28, 1579-1588.	2.8	14
38	NMDA and non-NMDA receptors stimulation causes differential oxidative stress in rat cortical slices. Neurochemistry International, 2006, 49, 475-480.	3.8	13
39	Role of Ongoing, Intrinsic Activity of Neuronal Populations for Quantitative Neuroimaging of Functional Magnetic Resonance Imaging–Based Networks. Brain Connectivity, 2011, 1, 185-193.	1.7	12
40	Distributions of Irritative Zones Are Related to Individual Alterations of Resting-State Networks in Focal Epilepsy. PLoS ONE, 2015, 10, e0134352.	2.5	12
41	Rhythmic 3–4Hz discharge is insufficient to produce cortical BOLD fMRI decreases in generalized seizures. Neurolmage, 2015, 109, 368-377.	4.2	11
42	Alterations of Parenchymal Microstructure, Neuronal Connectivity, and Cerebrovascular Resistance at Adolescence after Mild-to-Moderate Traumatic Brain Injury in Early Development. Journal of Neurotrauma, 2019, 36, 601-608.	3.4	11
43	Supraspinal Sensorimotor and Pain-Related Reorganization after a Hemicontusion Rat Cervical Spinal Cord Injury. Journal of Neurotrauma, 2021, 38, 3393-3405.	3.4	8
44	Small loci of astroglial glutamine synthetase deficiency in the postnatal brain cause epileptic seizures and impaired functional connectivity. Epilepsia, 2021, 62, 2858-2870.	5.1	7
45	Mapping phosphorylation rate of fluoro-deoxy-glucose in rat brain by 19F chemical shift imaging. Magnetic Resonance Imaging, 2014, 32, 305-313.	1.8	6
46	Spontaneous activity forms a foundation for odor-evoked activation maps in the rat olfactory bulb. NeuroImage, 2018, 172, 586-596.	4.2	6
47	Association Between Magnetic Resonance Imaging-Based Spinal Morphometry and Sensorimotor Behavior in a Hemicontusion Model of Incomplete Cervical Spinal Cord Injury in Rats. Brain Connectivity, 2020, 10, 479-489.	1.7	5
48	Thalamic activations in rat brain by fMRI during tactile (forepaw, whisker) and non-tactile (visual,) Tj ETQq0 0 0 rg	BT /Overlc	ocg 10 Tf 50
49	Fractal correlation structure in fMRI data of rat brain. Journal of Cerebral Blood Flow and Metabolism, 2005, 25, S379-S379.	4.3	1
50	Influence of volatile induction agents on fMRI and neural activity. Journal of Cerebral Blood Flow and Metabolism, 2005, 25, S395-S395.	4.3	1
51	Effects of isoflurane induction on inter-animal reproducibility. Journal of Cerebral Blood Flow and Metabolism, 2005, 25, S397-S397.	4.3	0
52	Effects of volatile agents on neurophysiology in α-chloralose anesthetized rats. Journal of Cerebral Blood Flow and Metabolism, 2005, 25, S200-S200.	4.3	0